Supplementary Information

Tough, Long-lasting Adhesive Hydrogel Patch Via the Synergy of Interfacial Entanglement and Densifying Adhesion Groups

Yunjie Lu, Zhaohui Li, Zewei Li, Shihao Zhou, Ning Zhang, Jianming Zhang and Lu Zong*

Key Laboratory of Rubber-Plastics, Ministry of Education/Shandong Provincial Key Laboratory of Rubber-Plastics, Qingdao University of Science & Technology, Qingdao City 266042, People's Republic of China

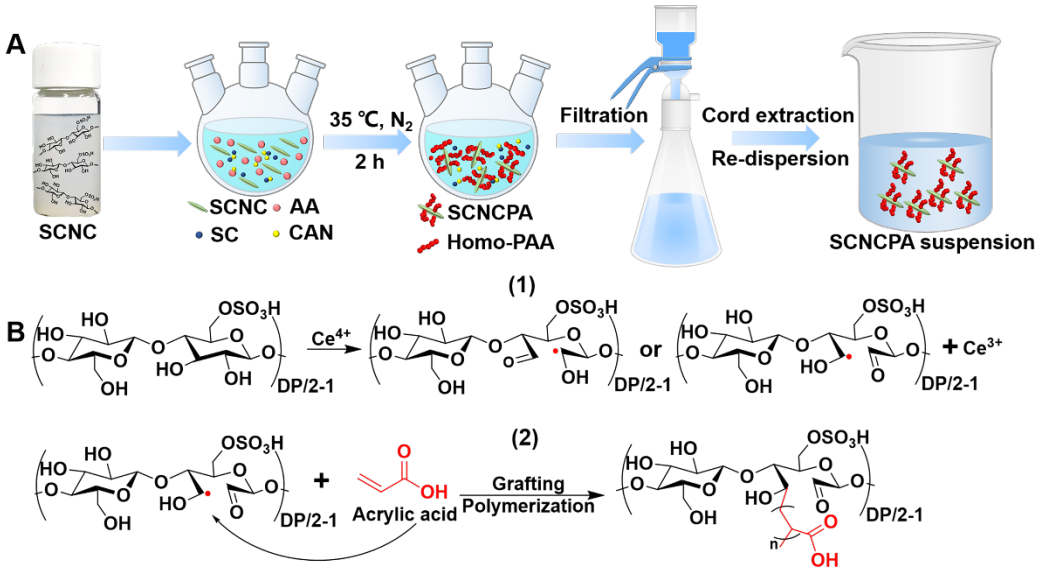

Fig. S1 Preparation process of SCNCPA. (A) Reaction steps for initiating graft polymerization of AA monomers on the surface of SCNC to obtain SCNCPA using a synergistic initiation system of ceric ammonium nitrate (CAN) and sodium citrate (SC). (B) Reaction equations for Ce^{4+} initiated grafting of SCNC and PAA. Ce^{4+} opens the ring at C_2, C_3 on the six-membered ring of SCNC through redox reaction and generates a free radical, which subsequently initiated the free radical polymerization of AA monomer at this point, while the obtained PAA molecular chain was grafted onto the surface of SCNC.

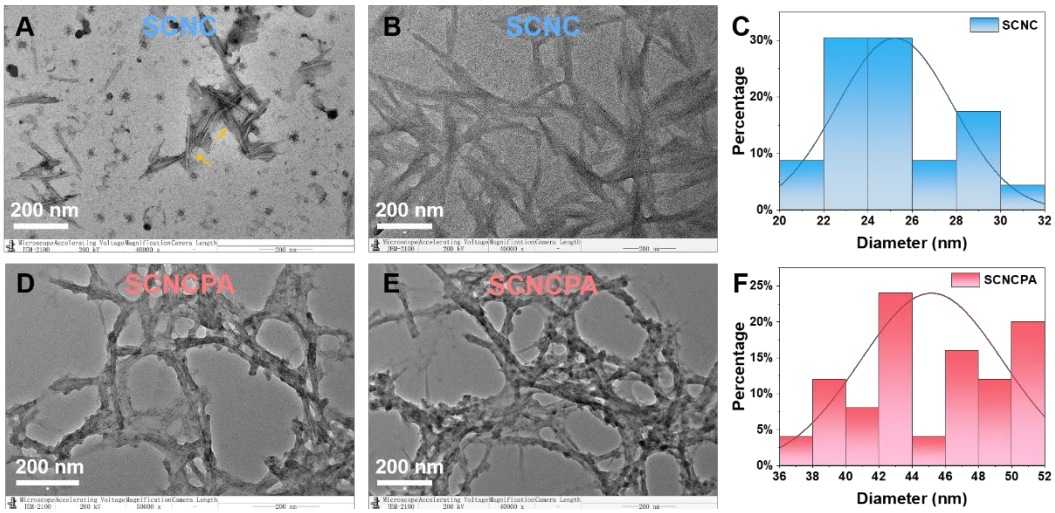

Fig. S2 TEM images of SCNC, SCNCPA. (A) TEM images of SCNC stained with 2% phosphotungstic acid solution at a magnification of 40000x. It can be seen that there is a tendency for SCNC or SCNCPA to lap or aggregate with each other due to the easy formation of hydrogen bonds between the surface polar groups. (B) TEM images of SCNC with a magnification of 40,000x. (C) Size statistics of the nanoparticles in B. (D, E) TEM images of SCNCPA. F Size statistics of the nanoparticles in E.

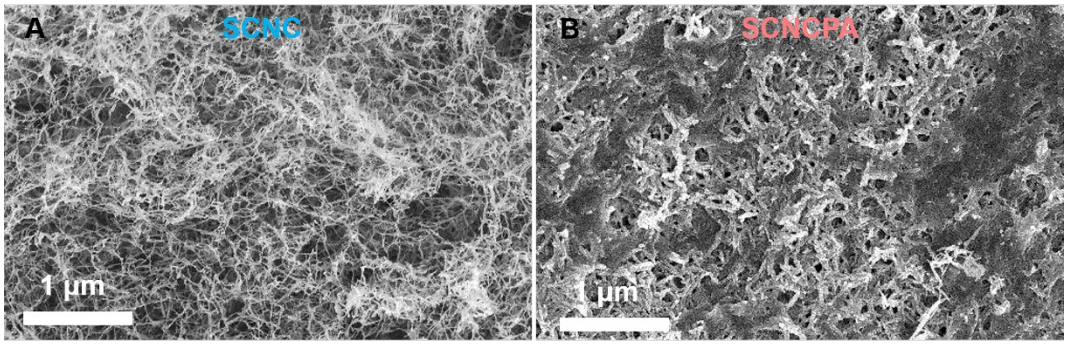

Fig. S3 SEM images of SCNC, SCNCPA freeze-dried powders. (A) SCNC. (B) SCNCPA.

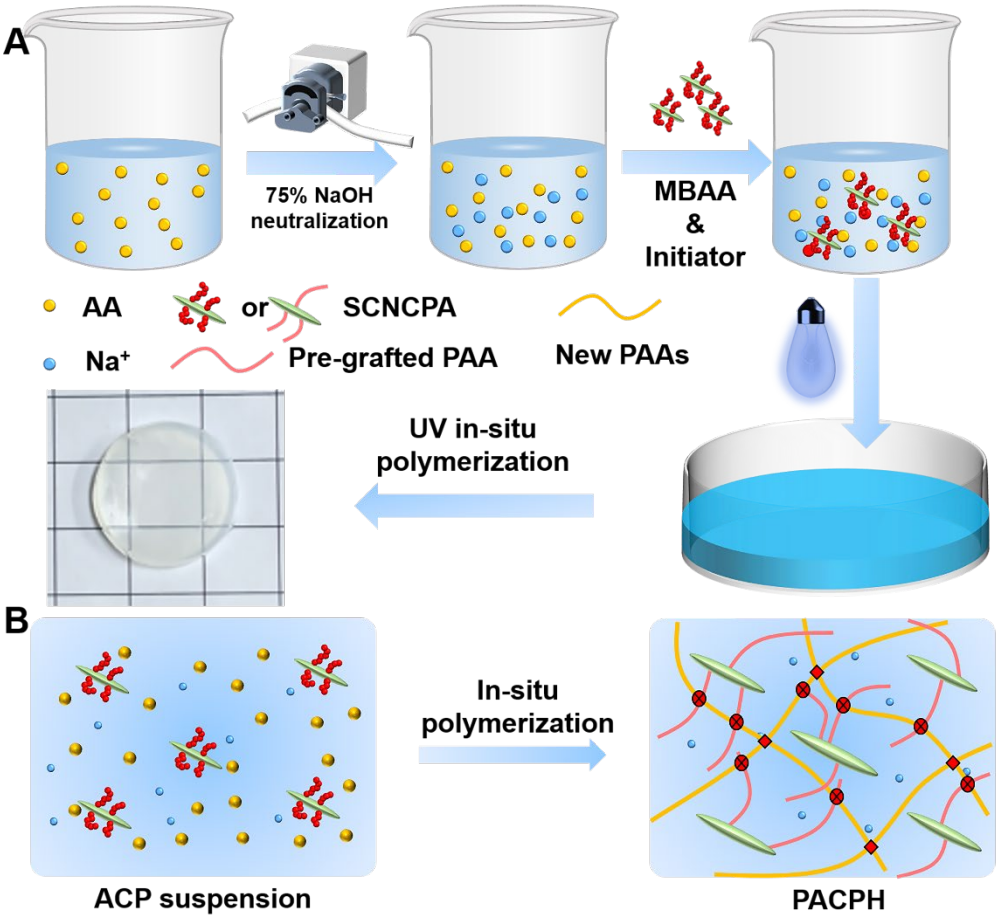

Fig. S4 Preparation steps and microstructure schematic of PACPH hydrogel. (A) Preparation steps for the preparation of PACPH hydrogels using SCNCPA as a nano-reinforcing and adhesion-enhancing material. (B) Schematic diagram of the interactions between SCNCPA and the hydrogel molecular chain network inside the PACPH hydrogels obtained by *in-situ* polymerization under UV radiation.

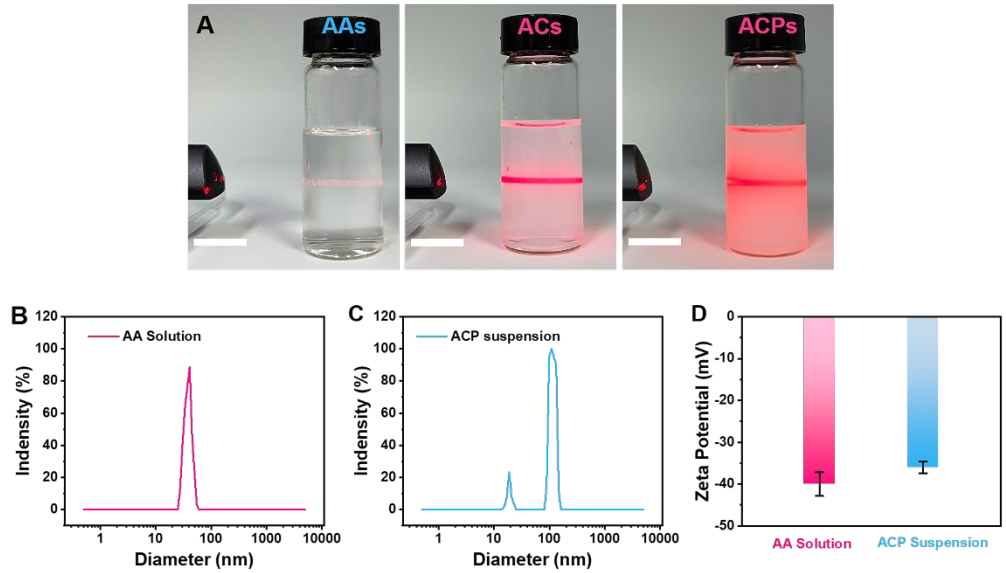

Fig. S5 Dispersibility and stability of SCNCPA. (A) Precursor solution (from left to right, AA/NaOH (neutralized 75%, AAs), AA/NaOH/SCNC (ACs), AA/NaOH/SCNCPA (ACPs)). (B) Dynamic light scattering (DLS) curves for AAs. (C) DLS curves for ACPs. (D) Zeta potentials of AAs and ACPs.

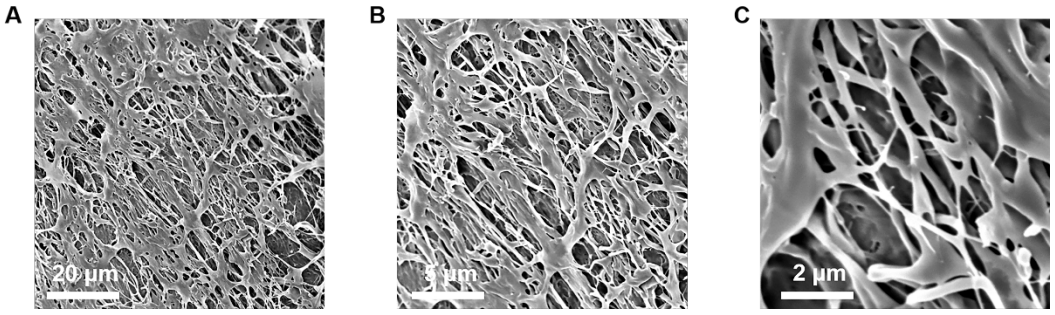

Fig. S6 SEM image of PAAH hydrogel after freeze-drying at different magnifications.

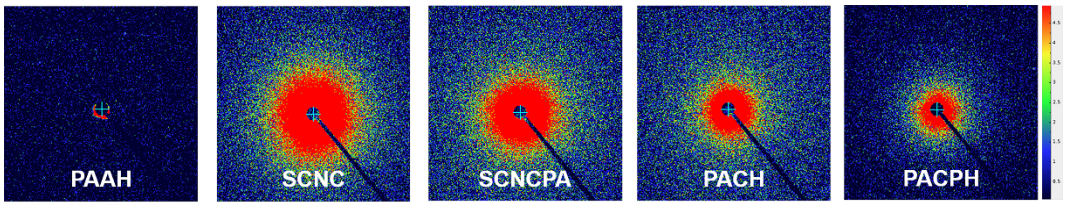

Fig. S7 Two-dimensional small-angle scattering spectra of SCNC, SCNCPA, PAAH, PACH, and PACPH.

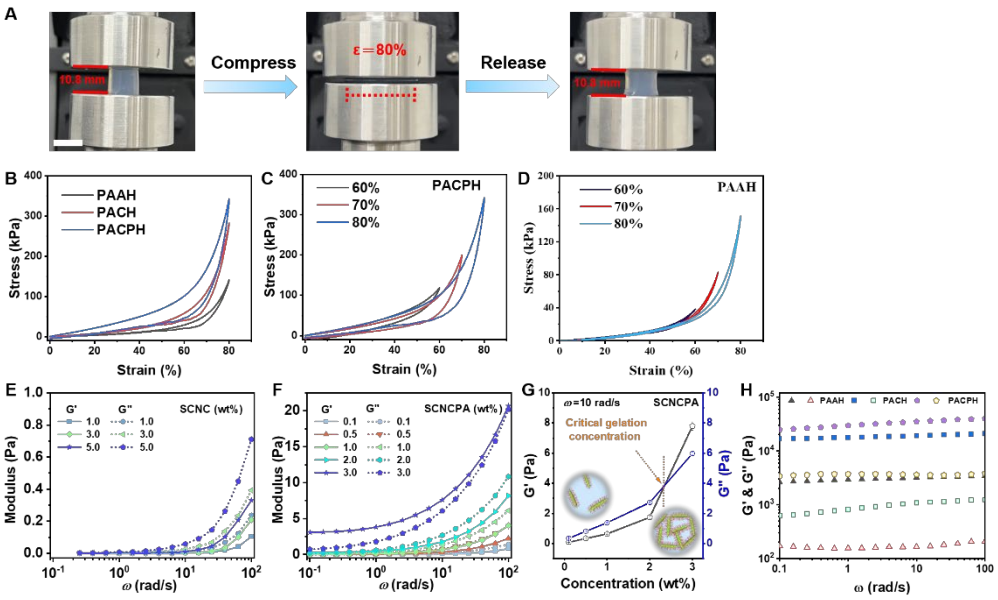

Fig. S8 Compression properties of PACPH hydrogel. (A) Physical picture of compression and recovery of PACPH. (B) Compression cycling curves of PAAH, PACH, and PACPH. (C, D) Compression cycling curves of PACPH and PAAH hydrogels at different compression ratios. (E, F) Rheological profiles of SCNC and SCNCPA suspensions with different concentrations. (G) Curves of energy storage modulus G' and loss modulus G'' versus variation with concentration for SCNCPA suspensions at ω = 10 rad/s. (H) Rheological properties of PAAH, PACH, PACPH, trends of energy storage modulus G' (solid), loss modulus G'' (hollow) with frequency.

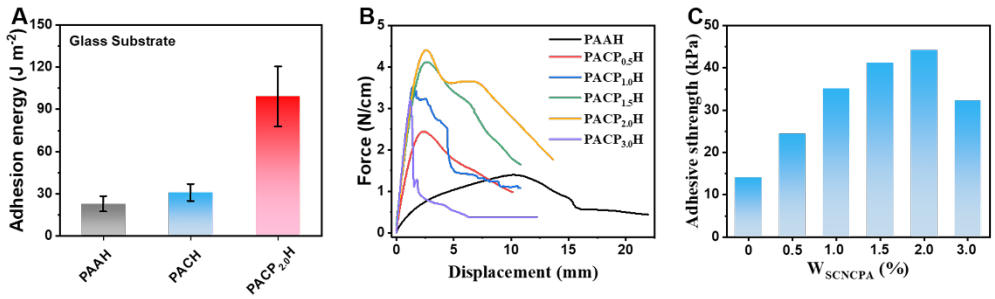

Fig. S9 (A) Interfacial adhesion energies obtained by integration of F-X curves for PAAH, PACH, and PACPH. (B, C) Adhesion curves (F-X curves) and adhesion strengths of PACPXH to glass substrates with different SCNCPA contents.

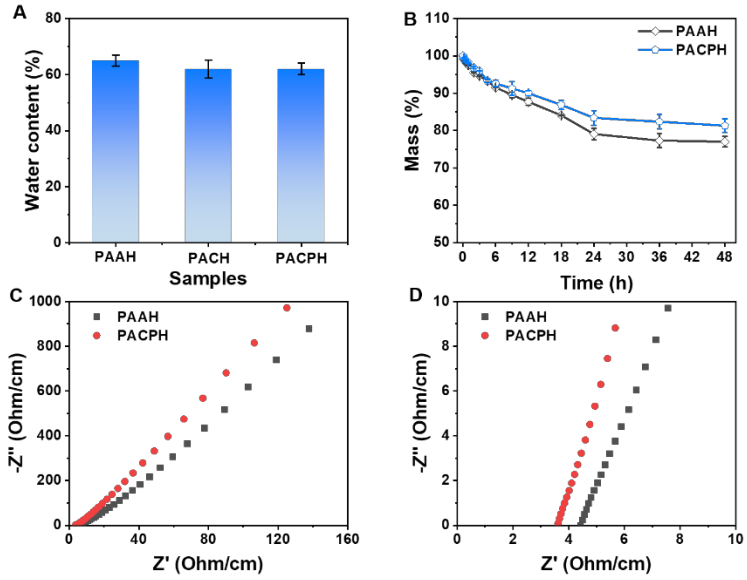

Fig. S10 Water content (A) and water retention properties (B) of PAAH, PACH, PACPH. (C) EIS Nyquist plots of ion-conducting hydrogels PAAH and PACPH. (D) Localized enlargement of C plots.

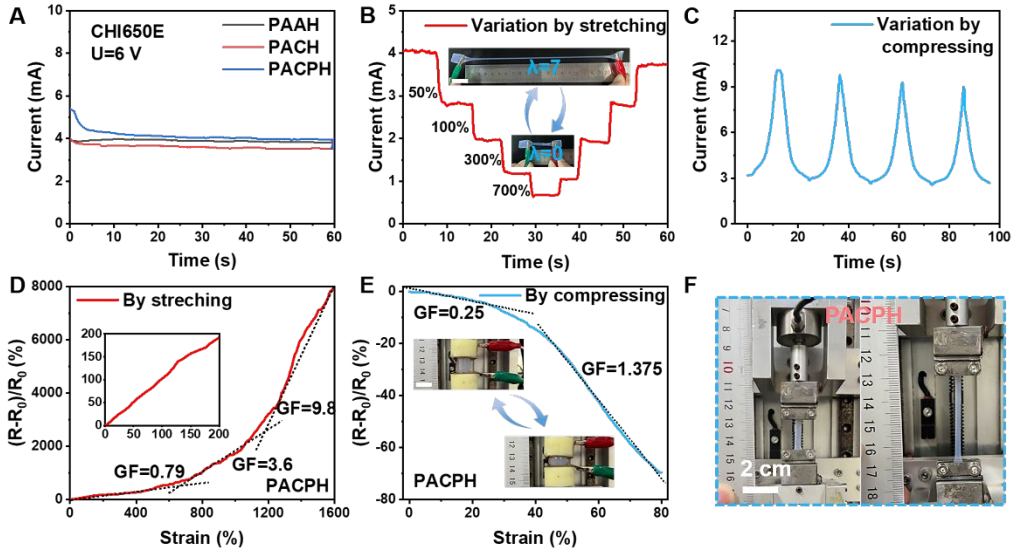

Fig. S11 Conductivity and strain sensing. (A) The electrical conductivity of PAAH, PACH, and PACPH at constant voltage. (B) Current variation of PACPH stretched to different multiplications at constant voltage. (C) Current variation of PACPH during cyclic compression (60% of compression deformation). (D) Resistance variation under continuous stretching to 1600% deformation. During stretching, at small strains, the degree of change in the internal network structure with stretching is low, and the network remains in a sparse state, slower change in ion mobility rate, and thus the rate of change in ionic conductivity is low. However, at large strains, the internal network structure becomes progressively denser with stretching, ion migration is hindered, and the ionic conductivity decreases sharply. (E) Resistance variation under continuous compression to 80% deformation. (F) Pictures of PACPH in the cyclic stretching process.

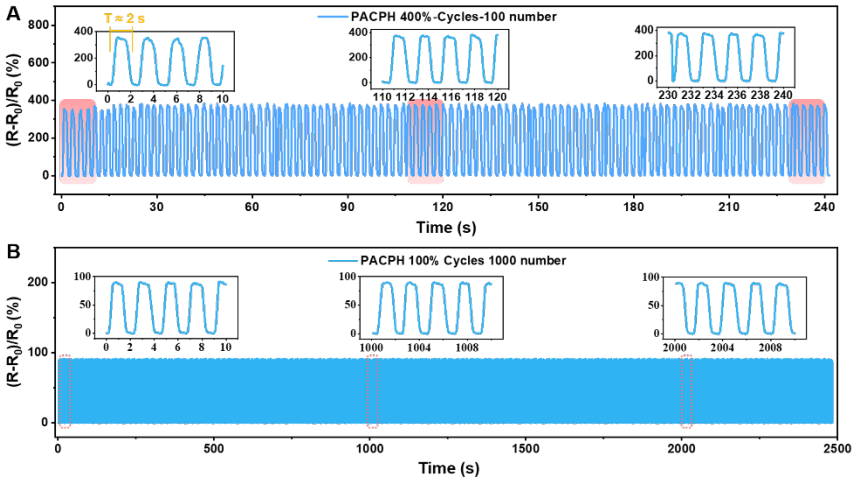

Fig. S12 Strain sensing performance under different deformations. (A) Resistance change during 100 cycles of stretching at large strain (400%), the insets are T=0-10, 110-120, 230-240 s, from which it can be seen that PACPH has stable sensing performance even at large deformation. (B) Resistance change during 1000 cycles of stretching at small strain (100%), the insets are T=0-10, 1000-1010, 2000-2010 s.

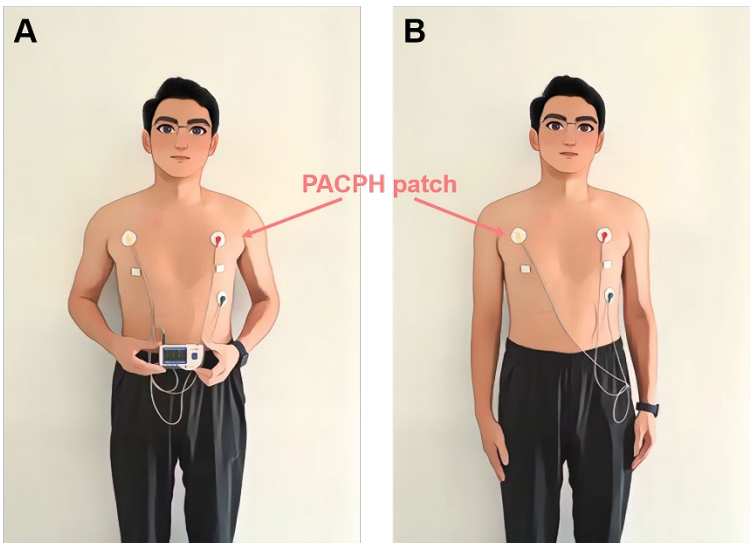

Fig. S13 Schematic diagram of the operation of the PACPH ECG electrode patch. (A) Monitoring of ECG signals, position of the PACPH patch on the human body. (B) Schematic diagram of the monitoring of ECG signals in the exercise state.

Fig. S14 (A-E) The PACPH patch is connected to the button electrodes and attached to the designated location on the human body, and then connected to the signal receiving device to monitoring the ECG signals of the human body in real time under different exercise states and different times of the day. (F) After attaching the PACPH patch, the human body's heart rate changes in the continuous one-day monitoring.